

Hydrogen Permeation and Electrochemical Corrosion Behavior of the X80 Pipeline Steel Weld

H.B. Xue and Y.F. Cheng

(Submitted July 30, 2011; in revised form January 9, 2012; published online April 18, 2012)

In this work, the microstructure of an X80 pipeline steel weld was characterized by optical and scanning electron microscopy. The hydrogen permeation and electrochemical corrosion behavior were investigated by various electrochemical measurements and analysis. It was found that there is the smallest hydrogen permeation rate, but the largest hydrogen trapping density at heat-affected zone, while the base steel has the lowest hydrogen trapping. These results are associated with the typical microstructure of the individual zone. Moreover, the accumulation of hydrogen atoms would result in an enhanced corrosion locally.

Keywords corrosion, hydrogen permeation, microstructure, weld, X80 steel

1. Introduction

Corrosion has been a vital problem affecting the safe operation and integrity of oil/gas pipelines (Ref 1, 2). Field observations found (Ref 1) that pipeline corrosion occurs preferentially at the welding area. It was believed (Ref 3, 4) that welding would increase the electrochemical corrosion activity of the steel locally due to the metallurgical effect and residual stresses introduced.

Hydrogen could be introduced into steel during welding (Ref 5). After solidification of weld, the atomic hydrogen is retained, diffusing through the weld metal and heat-affected zone (HAZ), and being trapped at various metallurgical defects, such as dislocations, voids, grain boundaries, and inclusions (Ref 6, 7). Hydrogen-enhanced localized corrosion has been the potential reason that causes failure of welded high-strength steels.

The electrochemical hydrogen permeation test provides an alternative to understand the hydrogen-steel interaction. It enables the quantitative determination of the important properties, such as hydrogen permeating flux, the concentration of hydrogen, hydrogen diffusivity, etc. (Ref 8, 9). Moreover, the photo-electrochemical technique is capable of characterizing in situ the effect of hydrogen on corrosion of the steel (Ref 10–13). For example, Maffi et al. (Ref 13) used a scanning photo-electrochemical microscopy to image the spatial distribution of hydrogen in A516 steel, and concluded that the welded region has a high concentration of hydrogen trapped than the other regions.

High-strength pipeline steel, such as X80 steel, has been used in the new pipeline projects. There has been so far limited work investigating the combined effect of hydrogen and the steel metallurgy on local corrosion at weld. In this work, the microstructure of the welding zones, including the weld metal, HAZ, and base steel, on a X80 steel was characterized by optical and scanning electron microscopy (SEM). The hydrogen permeation characteristics were determined by electrochemical hydrogen permeation tests. The effect of hydrogen on local corrosion at the steel weld was studied by photo-electrochemical and polarization curve measurements.

2. Experimental

2.1 Material and Metallographic Characterization

Specimens used in this work were cut from a sheet of longitudinally welded X80 steel pipe, with a chemical composition (wt.%): C 0.07, Mn 1.86, Si 0.27, Cr 0.04, Mo 0.3, Cu 0.27, Al 0.026, S 0.01, P 0.015, Ti 0.01, Nb 0.079, and Fe balance. The welded segment of the steel pipe was machined into a flat specimen, as shown in Fig. 1. The specimen was ground sequentially to 1200 grit SiC paper, polished with 1 μm diamond paste. The specimen was etched in Nital solution, i.e., a mixture of 4% nitric acid and ethanol, for metallographic characterization.

The microstructure of the base steel, HAZ, and the weld metal was characterized by using an optical microscope and a Model Philips XL30 SEM.

2.2 Electrochemical Hydrogen Permeation Measurement

The electrochemical hydrogen permeation test was carried out using a modified *Devanathan-Stachurski* cell (Ref 14). Specimens cutting from base steel, HAZ, and the weld metal were installed between the two cells, with an exposed area of 50 mm² and a thickness of 0.5 mm. The hydrogen-charging cell was filled with 0.5 M H₂SO₄ solution, and a constant cathodic current density of 10 mA/cm² was applied. The hydrogen-detecting cell contained 0.1 M NaOH solution under an anodic potential of 200 mV(SCE). Prior to test, the cells were purged with a high-purity nitrogen gas (99.99%) for 2 h to

H.B. Xue and Y.F. Cheng, Department of Mechanical Engineering, University of Calgary, 2500 University Drive NW, Calgary, AB T2N 1N4, Canada. Contact e-mail: fcheng@ucalgary.ca.

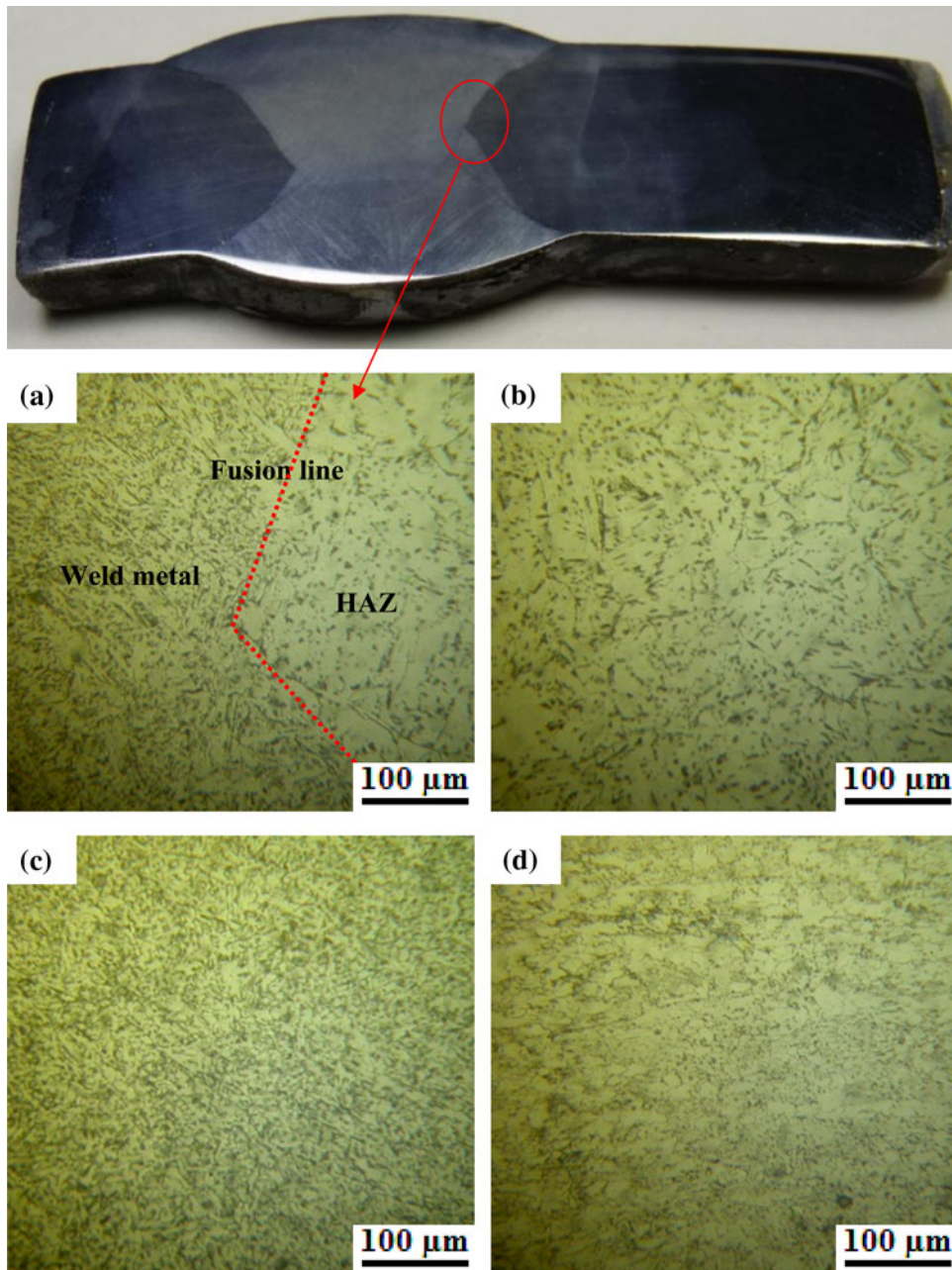


Fig. 1 Optical views of the microstructure of the welded X80 pipeline steel (a) HAZ/weld metal, (b) HAZ, (c) weld metal, and (d) base steel

remove the dissolved oxygen from solutions. The hydrogen permeation current measurement was conducted through a Reference 600 Gamry electrochemical system and a PARSTAT 263A potentiostat.

2.3 Hydrogen Permeation Current Analysis

The hydrogen permeating flux, J_H , through the steel specimen ($\text{mol H/m}^2 \text{ s}$) was measured by the steady-state hydrogen permeation current density, i_p^∞ (Ref 15):

$$J_H = \frac{i_p^\infty}{nF} \quad (\text{Eq 1})$$

where n is the number of electrons transferred, and F is Faraday's constant. The hydrogen permeation rate (mol H/m s) is defined by:

$$J_H L = \frac{i_p^\infty L}{nF} \quad (\text{Eq 2})$$

where L is the specimen thickness. The effective hydrogen diffusivity, D_{eff} , can be calculated by (Ref 16, 17):

$$D_{\text{eff}} = \frac{L^2}{6t_L} \quad (\text{Eq 3})$$

where t_L is the time-lag, corresponding to the point on the hydrogen permeation current curve at which $i_t = 0.63i_p^\infty$. The subsurface concentration of hydrogen, C_H , (mol H/m^3) is defined by:

$$C_H = \frac{J_H L}{D_{\text{eff}}} \quad (\text{Eq 4})$$

2.4 Polarization Curve Measurement

Measurement of polarization curve of the steel electrode was performed in NS4 solution using the identical cell to that for photocurrent measurement. The solution contained 0.483 g/l NaHCO_3 , 0.122 g/l KCl , 0.181 g/l $\text{CaCl}_2 \cdot 2\text{H}_2\text{O}$, and 0.131 g/l $\text{MgSO}_4 \cdot 7\text{H}_2\text{O}$. The potential scanning rate was 0.3 mV/s, and the scanning range was from -1200 to 400 mV(SCE).

3. Results

3.1 Metallographic Characterization

Figure 1 shows the optical view of the microstructure of various zones at X80 steel weld. It is seen that the weld metal, fusion line, and HAZ were present clearly in Fig. 1(a), and featured with different microstructures. To further characterize the welding zone's microstructure, the metallographic feature was observed by SEM and the views are shown in Fig. 2. The HAZ (Fig. 2b) contained a mixture of bainite (B) and ferrite (F) with the white cementite (C). The weld metal was featured with acicular ferrite (AF) and grain boundary ferrite (GBF), as shown in Fig. 2(c). The microstructure of X80 steel (Fig. 2d) contained typically polygonal ferrite and bainite bundles.

3.2 Electrochemical Hydrogen Permeation Tests

Figure 3 shows the hydrogen permeation current curves measured on the weld metal, HAZ, and base steel specimens,

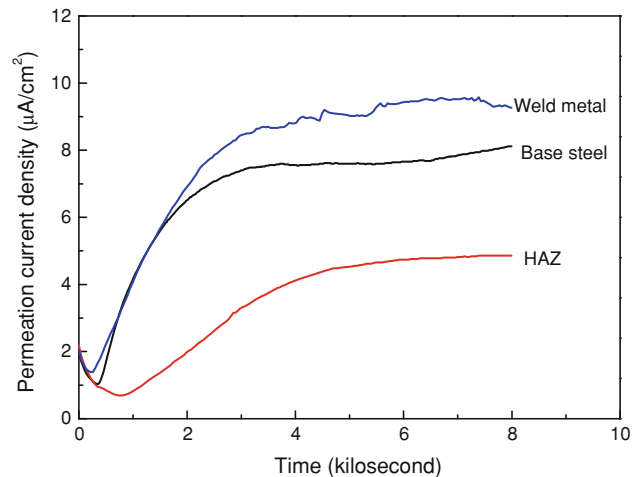


Fig. 3 Hydrogen permeation current density curves measured at various zones of the weld under a cathodic charging current density of 10 mA/cm^2 in $0.5 \text{ M H}_2\text{SO}_4$ solution

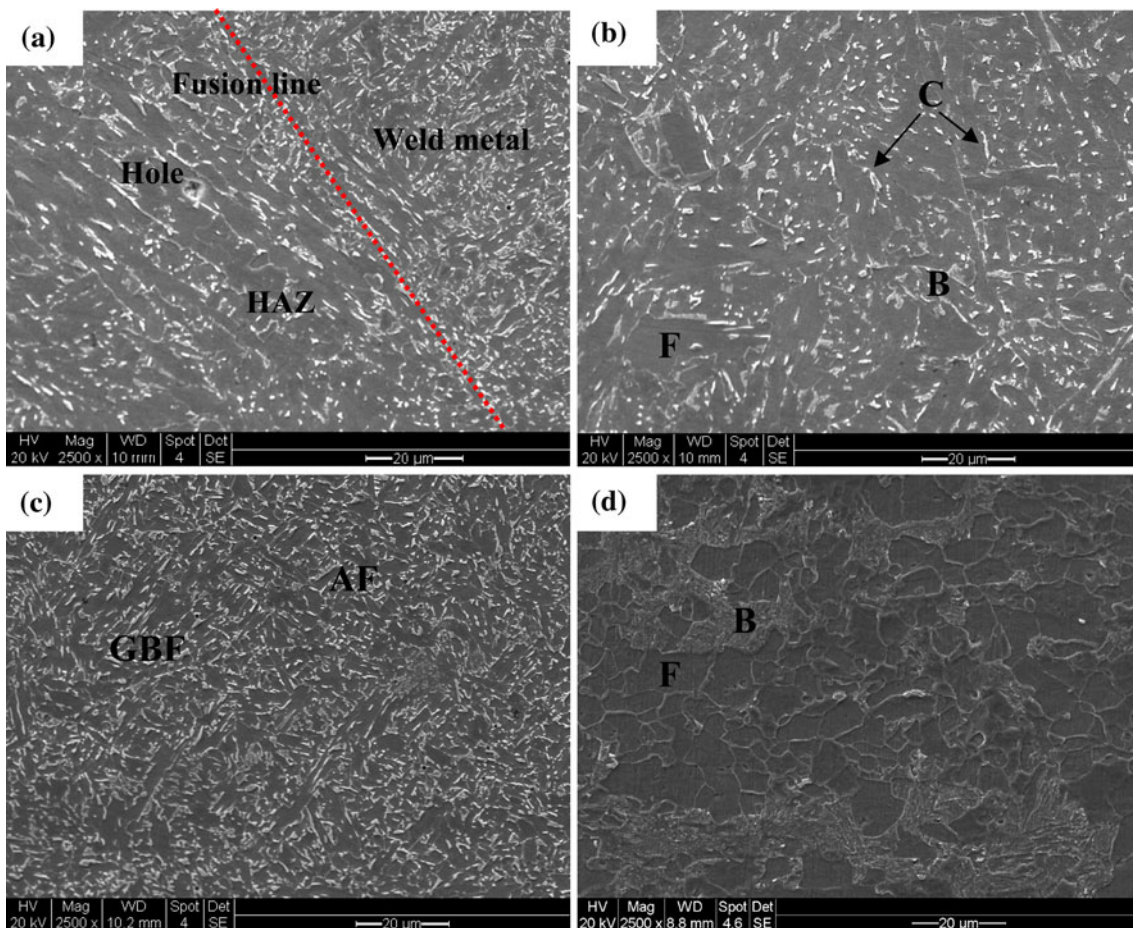


Fig. 2 SEM observation of the microstructure of the welded X80 steel (a) HAZ/weld metal, (b) HAZ, (c) weld metal, and (d) base steel

respectively, under a cathodic current density of 10 mA/cm² in 0.5 M H₂SO₄ solution. It is seen that, after a break-through time, the hydrogen permeation current increased with time, and then reached a relatively steady value. Moreover, the steady-state hydrogen permeation current density measured on the weld metal was higher than that of base steel. There was the smallest permeation current density at HAZ.

3.3 Polarization Curve Measurements

Figure 4 shows the polarization curves measured on the uncharged and charged weld metal, HAZ and base steel electrodes in NS4 solution. It is seen that, at individual anodic potential, the anodic current density measured on the three zones was ranked as: HAZ > base steel > weld metal in the absence and presence of hydrogen-charging. Moreover, at each zone, the anodic current density of the charged steel electrode was higher than that of the uncharged one under individual potential.

3.4 Microstructural Characterization upon Hydrogen-Charging

Figure 5 shows the local preferential corrosion observed around the fusion zone of the welded X80 steel specimen upon

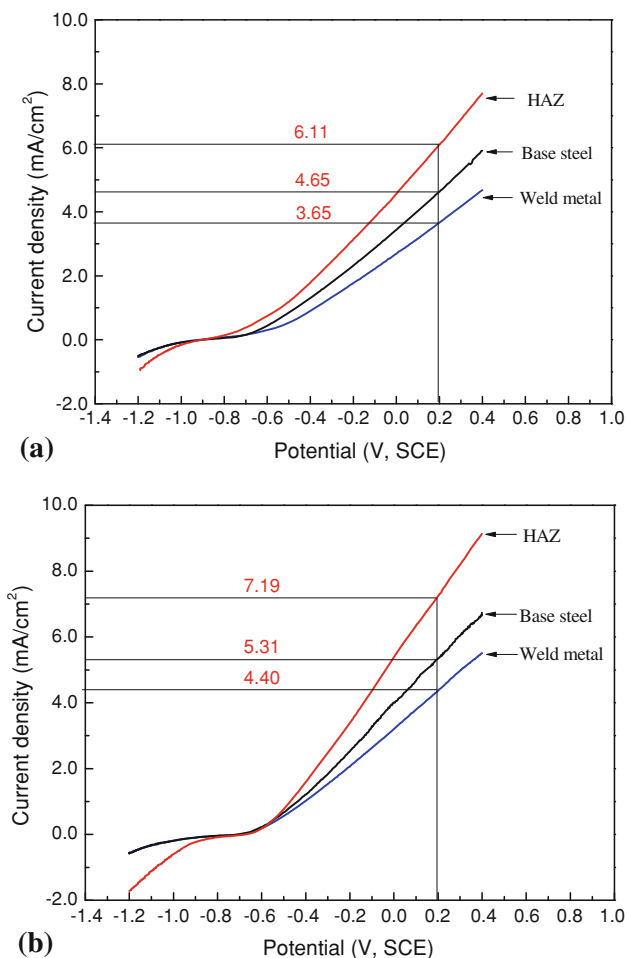


Fig. 4 Polarization curves measured at various zones of the weld in NS4 solution in the absence (a) and presence (b) of hydrogen-charging at cathodic current density of 10 mA/cm² for 2 hours

hydrogen-charging. It is seen that corrosion was associated with inclusions A, B, and C that were located in the weld metal and HAZ zones.

Figure 6 shows the EDXA spectra of the inclusions. The inclusions were primarily enriched in Si (Fig. 6a and c) and Al-Si (Fig. 6b).

4. Discussion

4.1 Hydrogen Permeation Behavior of X80 Steel Weld

The fundamentals of the hydrogen permeation into steel can be determined by measurement of the hydrogen permeation current (Fig. 3) and the numerical calculations by Eq 1-4. Moreover, the hydrogen trapping density in the steel can be estimated by (Ref 18):

$$N_T = \frac{S_{app}}{3} \left(\frac{D_l}{D_{eff}} - 1 \right) \quad (\text{Eq 5})$$

where N_T is the number of hydrogen trapping sites per unit volume of the steel (m⁻³), S_{app} is the apparent solubility of hydrogen (mol H/m³), and D_l is the lattice diffusion coefficient of hydrogen (m²/s), with a value of 1.28×10^{-8} m²/s in α -Fe (Ref 6). This value is used in this work due to the unavailability of this parameter for X80 steel.

Table 1 shows the determined values of the hydrogen permeation rate, diffusivity of hydrogen, and the trapping density at the weld metal, HAZ, and the base steel, respectively. In particular, there is the smallest hydrogen permeation rate at HAZ, and it contains most hydrogen traps. This is probably due to the presence of cementite (Fe₃C) precipitates, which act as the obstacle for the hydrogen transport (Ref 19). Since the hydrogen trapping density is relatively high, and some may distribute on the subsurface of the steel, the hydrogen subsurface concentration at HAZ is thus not low.

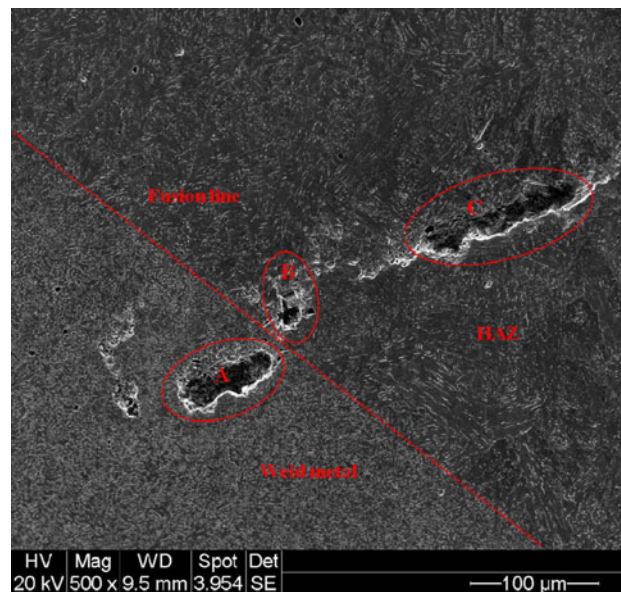


Fig. 5 Hydrogen induced cracks around the fusion zone of the weld

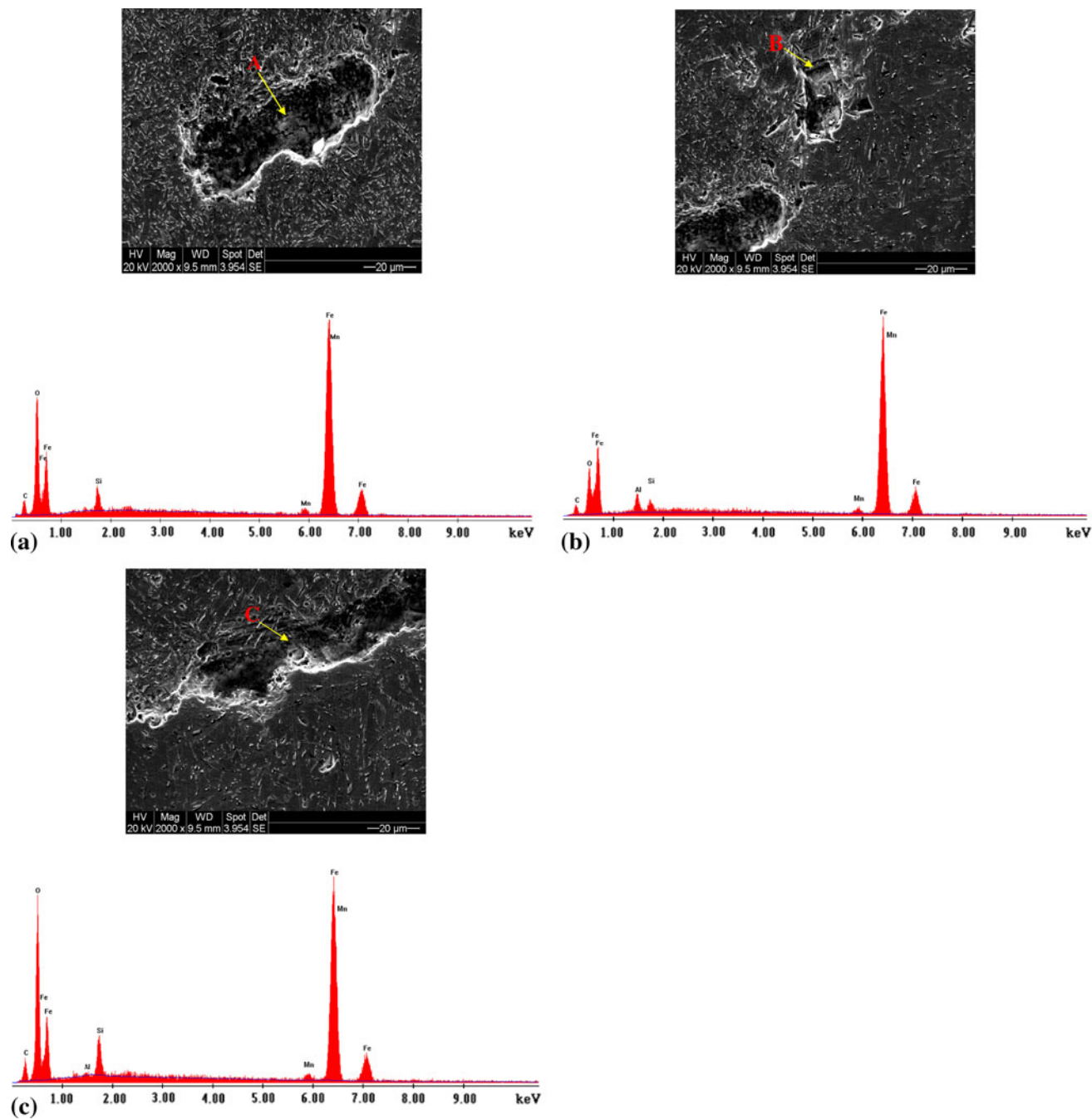


Fig. 6 The hydrogen-induced cracks initiated at inclusions and the EDX spectra obtained at the individual inclusion

Table 1 The fitted results from the hydrogen permeation current density curves, including hydrogen permeation rate ($J_{H,L}$), diffusivity of hydrogen (D_{eff}), subsurface concentration of hydrogen (C_H), and the trapping density (N_T) in various zones of the weld

Weldment zone	$J_{H,L}$, mol H/m s	D_{eff} , m ² /s	C_H , mol H/m ³	N_T , m ⁻³
Weld metal	4.74×10^{-10}	2.72×10^{-11}	17.43	1.64×10^{27}
HAZ	2.49×10^{-10}	1.49×10^{-11}	16.71	2.88×10^{27}
Base steel	4.06×10^{-10}	3.35×10^{-11}	12.12	0.93×10^{27}

The base X80 steel with a polygonal ferrite and bainitic ferrite (Fig. 2d) has the highest hydrogen diffusivity and a low hydrogen subsurface concentration. This is attributed to the

diffusion paths existing along the grain boundaries in ferrite (Ref 20). Moreover, the hydrogen trapping density in X80 steel is very low, indicating the steel is quite “clean”.

4.2 Hydrogen Trapping and the Hydrogen-Enhanced Corrosion of Steel

The polarization curve measurements (Fig. 4) show that hydrogen-charging enhances the anodic dissolution current density of the steel, as demonstrated in previous work (Ref 21). Moreover, there is the highest anodic current density at HAZ, indicating that HAZ is associated with the high electrochemical activity in the solution. Upon hydrogen-charging, hydrogen would be trapped in HAZ at sites such as grain boundaries and the phase interfaces as well as inclusions. The hydrogen permeation analysis shows that there exist a significant number of various traps in HAZ (there is the highest trapped density at HAZ in Table 1). Of various traps, the presence of irreversible traps, such as inclusions, is important since hydrogen trapped at these sites is directly associated with an enhanced local, preferential corrosion. As indicated in the present work in Fig. 5, the local corrosion occurs preferentially at inclusions existing at HAZ.

Furthermore, this work finds that the hydrogen-enhanced localized corrosion occurs primarily at inclusions enriching in Si and Si-Al, as seen in Fig. 6. The author's previous work (Ref 22) demonstrated that there exist different electrochemical activities between inclusion and the steel substrate. In particular, the Si-enriched inclusion is more active than the steel. In corrosive solutions, a preferential dissolution of inclusion would occur at the steel/inclusion interface. When hydrogen is trapped there, local dissolution would be further enhanced. Therefore, local corrosion pits or dissolution-induced flaws are observed at inclusions.

5. Conclusions

There are different microstructures at the X80 steel weld. The HAZ contains a mixture of bainite and ferrite as well as randomly distributed cementite. The weld metal is featured with acicular ferrite and grain boundary ferrite, and the microstructure of X80 steel contains typically polygonal ferrite and bainite bundles.

The microstructure of the weld zone results in different hydrogen permeation behavior. There is the smallest hydrogen permeation rate and the highest hydrogen trapping density at HAZ, while the base X80 steel has the lowest hydrogen trapping density.

Hydrogen-charging enhances corrosion of the steel, especially localized corrosion occurring at HAZ. This is probably due to the high hydrogen trapping density at HAZ, accumulating hydrogen locally to cause the preferential dissolution.

Acknowledgments

This work was supported by Canada Research Chairs Program and Natural Science and Engineering Research Council of Canada (NSERC).

References

1. R.N. Parkins, A Review of Stress Corrosion Cracking of High-Pressure Gas Pipelines, *Corrosion'2000*, NACE, Houston, TX, 2000, Paper No. 363
2. F. King, T.R. Jack, W. Chen, S.H. Wang, M. Elboujdaini, W. Revie, R. Worthingham, and P. Dusek, Development of Predictive Model for the Initiation and Early-Stage Growth of Near-Neutral pH SCC of Pipeline Steels, *Corrosion'2001*, NACE, Houston, TX, 2001, Paper No. 1214
3. C. Zhang and Y.F. Cheng, Corrosion of Welded X100 Pipeline Steel in a Near-Neutral pH Solution, *J. Mater. Eng. Perform.*, 2010, **19**, p 834–840
4. B. Lu, J. Luo, and D. Ivey, Near-Neutral pH Stress Corrosion Cracking Susceptibility of Plastically Prestrained X70 Steel Weldment, *Metall. Mater. Trans. A*, 2010, **41A**, p 2538–2547
5. M. Law and D. Nolan, Fatigue Crack Growth Comparison Between Sleeved and Non-Sleeved Pipeline, *Adv. Mater. Res.*, 2008, **41–42**, p 105–112
6. R.A. Oriani, J.P. Hirth, and M. Smailowski, *Hydrogen Degradation of Ferrous Alloys*, Noyes Publications, Park Ridge, NJ, 1985
7. M. Law, D. Nolan, and R. Holdstock, Method for the Quantitative Assessment of Transverse Weld Metal Hydrogen Cracking, *Mater. Charact.*, 2008, **59**, p 991–997
8. P. Manolatos, C. Duret-Thual, J.L.E. Coze, M. Jerome, and E. Bollinger, The Electrochemical Permeation of Hydrogen in Steels without Palladium Coating. Part II: Study of the Influence of Microstructure on Hydrogen Diffusion, *Corros. Sci.*, 1995, **37**, p 1785–1796
9. M.A. Arafin and J.A. Szpunar, Effect of Bainitic Microstructure on the Susceptibility of Pipeline Steels to Hydrogen Induced Cracking, *Mater. Sci. Eng., A*, 2011, **528**, p 4927–4940
10. G. Razzini, M. Cabrini, S. Maffi, G. Mussati, and L. Peraldo Bicelli, Photoelectrochemical Visualization in Real-Time of Hydrogen Distribution in Plastic Regions of Low-Carbon Steel, *Corros. Sci.*, 1999, **41**, p 203–209
11. G. Razzini, S. Maffi, G. Mussati, and L. Peraldo Bicelli, The Scanning Photoelectrochemical Microscopy of Diffusing Hydrogen into Metals, *Corros. Sci.*, 1995, **37**, p 1131–1139
12. G. Razzini, S. Maffi, G. Mussati, L. Peraldo Bicelli, and G. Mitsi, Photo-Electrochemical Imaging of Hydrogen-Induced Damage in Stainless Steel, *Corros. Sci.*, 1997, **39**, p 613–620
13. S. Maffi, C. Lenardi, and B. Bozzini, Photoelectrochemical Imaging of Non-Planar Surfaces: The Influence of Geometrical and Optical Factors on Image Formation, *Meas. Sci. Technol.*, 2002, **13**, p 1398–1403
14. H.B. Xue and Y.F. Cheng, Photo-Electrochemical Studies of the Local Dissolution of a Hydrogen-Charged X80 Steel at Crack-Tip in a Near-Neutral pH Solution, *Electrochim. Acta*, 2010, **55**, p 5670–5676
15. S.H. Wang, W.C. Luu, K.F. Ho, and J.K. Wu, Hydrogen Permeation in a Submerged Arc Weldment of TMCP Steel, *Mater. Chem. Phys.*, 2002, **77**, p 447–454
16. Y.F. Cheng, Analysis of Electrochemical Hydrogen Permeation through X-65 Pipeline Steel and Its Implications on Pipeline Stress Corrosion Cracking, *Int. J. Hydrogen Energy*, 2007, **32**, p 1269–1276
17. K. Banerjee and U.K. Chatterjee, Hydrogen Permeation and Hydrogen Content Under Cathodic Charging in HSLA 80 and HSLA 100 Steels, *Scripta Mater.*, 2001, **44**, p 213–216
18. S.K. Yen and I.B. Huang, Critical Hydrogen Concentration for Hydrogen-Induced Blistering on AISI, 430 Steel, *Mater. Chem. Phys.*, 2003, **80**, p 662–666
19. C.F. Dong, Z.Y. Liu, X.G. Li, and Y.F. Cheng, Effects of Hydrogen-Charging on the Susceptibility of X100 Pipeline Steel to Hydrogen-Induced Cracking, *Int. J. Hydrogen Energy*, 2009, **34**, p 9879–9884
20. C. Zhang and Y.F. Cheng, Synergistic Effects of Hydrogen and Stress on Corrosion of X100 Pipeline Steel in a Near-Neutral pH Solution, *J. Mater. Eng. Perform.*, 2010, **19**, p 1284–1289
21. M.C. Li and Y.F. Cheng, Mechanistic Investigation of Hydrogen-Enhanced Anodic Dissolution of X-70 Pipe Steel and Its Implication on Near-Neutral pH SCC of Pipelines, *Electrochim. Acta*, 2007, **52**, p 8111–8117
22. T.Y. Jin and Y.F. Cheng, In-Situ Characterization by Localized Electrochemical Impedance Spectroscopy of the Electrochemical Activity of Microscopic Inclusions in an X100 Steel, *Corros. Sci.*, 2011, **53**, p 850–853